IEEE Access
Multidisciplinary | Rapid Review | Open Access Journal

Received 4 March 2024, accepted 20 March 2024, date of publication 27 March 2024, date of current version 3 April 2024.

Digital Object Identifier 10.1109/ACCESS.2024.3382205

RESEARCH ARTICLE

Control of a Snake Robot With Proximity Sensors to Adapt for Two Variable Planes

SHUNTA SUYAMA[1], MIZUKI NAKAJIMA[2], (Member, IEEE), HIKARU ARITA[3], (Member, IEEE), AND MOTOYASU TANAKA[1], (Member, IEEE)

[1]Department of Mechanical and Intelligent Systems Engineering, The University of Electro-Communications, Tokyo 182-8585, Japan
[2]Department of Robotics and Mechatronics, School of Science and Technology for Future Life, Tokyo Denki University, Tokyo 120-8551, Japan
[3]Department of Mechanical Engineering, Faculty of Engineering, Kyushu University, Fukuoka 819-0395, Japan

Corresponding author: Shunta Suyama (shunta.suyama@rc.mce.uec.ac.jp)

This work was supported in part by the Japan Society for the Promotion of Science (JSPS) KAKENHI Grant Number JP21H01285.

ABSTRACT This paper proposes a control method for a snake robot to move between two planes amidst changing environmental conditions. The proposed approach uses a proximity sensor affixed to the robot to estimate its position and orientation relative to the plane. When the robot's wheels become ungrounded due to environmental fluctuations, the control mode seamlessly transitions from propulsion control to recovery control. During recovery control, the robot is controlled to ensure that the ungrounded wheels regain contact with the plane. The integration of sensor information, propulsion control, and recovery control enables the snake robot to effectively adapt to the dynamically changing environment and maintain locomotion. The effectiveness of the proposed methodology was confirmed through experiments employing a snake robot. The results validate the robot's capability to traverse variable planes by utilizing the estimated information of plane. Moreover, the snake robot successfully regained ground contact through recovery control, even when encountering instances of ungrounded wheels during propulsion. Thus, the findings substantiate the robot's ability to sustain propulsion by maintaining the wheels grounded.

INDEX TERMS Environmental change, kinematics, proximity sensor, snake robot, traversing two planes.

I. INTRODUCTION

A snake robot represents a robotic system characterized by an elongated body shape and numerous joints, mimicking the features of a biological snake. Snake robots can achieve diverse motions by exploiting these features. Consequently, snake robots are expected to play an active role in disaster sites with diverse terrain. Based on their propulsion mechanisms, snake robots can be classified into three categories: passive-wheel type [1], [2], [3], [4], [5], [6], [7], [8], [9], [10] non-wheel type [11], [12], [13], [14], [15], [16], [17] and active-wheel type [18], [19], [20], [21]. By leveraging these distinct robot types for specific purposes, snake robots can be adapted to a wide range of environments. Most of the prior research on snake robots primarily focused on planar movements [1], [2], [3], [4], [5]. Recently, there has been a growing emphasis on more complex three-dimensional environments, such as discontinuous environments like steps [6], [7], [8], [11], [18], [19], and curved environments like cylinders [9], [12], [13], [14]. Nevertheless, most of these studies are restricted to unchanged environments.

Mobile robots are used not only to search disaster sites but also for transportation tasks and to explore extreme environments [22], [23]. However, when mobile robots perform transportation tasks in unknown outdoor terrain, they may encounter unexpected obstacles such as steps or uneven terrain. When they explore extreme environments, they may move on soft ground environments with variable terrain, such as snow and sand. Thus, there are many variable terrains in the real environment. Consequently, mobile robots need to adapt to changes in the environment to effectively operate in such environments.

Typical examples of mobile robots include leg-type [24], [25], [26], wheel-type [22], [23], [27], [28], [29], and

The associate editor coordinating the review of this manuscript and approving it for publication was Guilin Yang.

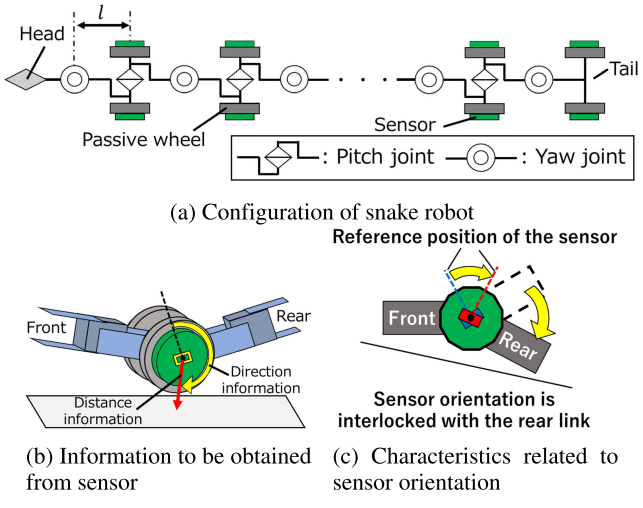

(a) Configuration of snake robot

(b) Information to be obtained from sensor

(c) Characteristics related to sensor orientation

FIGURE 1. Model of control object.

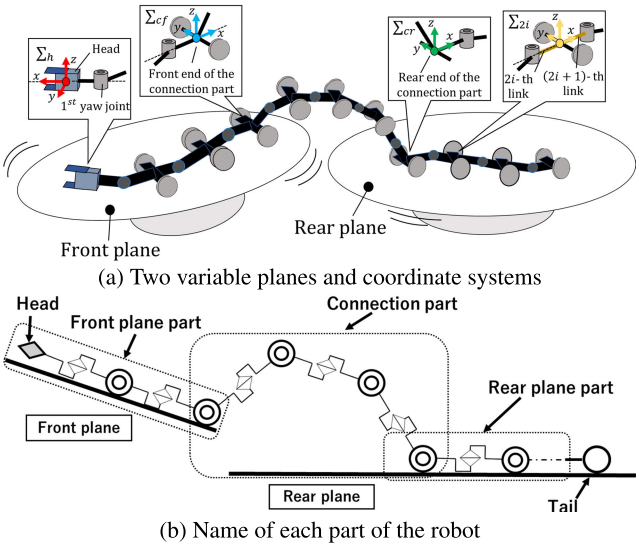

(a) Two variable planes and coordinate systems

(b) Name of each part of the robot

FIGURE 2. Assumed environment.

crawler-type robots [30], [31], [32]. Approaches that enable robots to adapt to variable terrains can be categorized into two types: mechanical solutions [24], [27], [30]], and control solutions [25], [26], [28], [29], [31], [32]. However, these approaches cannot be directly applied to snake robots because of their different mechanisms and principles of movement.

In the case of snake robots, as a mechanical solution, Bae et al. proposed a mechanism to assist snake robots in moving across uneven terrains [17]. Furthermore, Kouno et al. improved the mobility of an active-wheel-type snake robot on uneven terrains [20].

As an example of control solutions, Takemori et al. introduced a motion in which the entire body of the robot behaves akin to a crawler belt, thereby allowing the snake robot to move across the rubble [13]. Takemori et al. presented a control method that enables a snake robot to autonomously adapt to pipes with irregularly varying cross-sectional shapes [14]. Gong et al. proposed a method for a snake robot to adapt to the changing slope by estimating the angle of the slope [15]. Watanabe et al. proposed a rope-climbing motion for a snake robot utilizing rope deformation [16].

However, most of these studies focused on non-wheeled type snake robots, which rely on direct contact between the robot's body and the environment to move. This movement principle differs from wheel-type snake robots, which generate propulsive force through the interaction between the wheels and the environment. Consequently, the locomotion method for non-wheeled snake robots cannot be applied to wheeled snake robots. Kon et al. proposed a control method for a passive-wheel-type snake robot to ascend unknown steps using sensor information [6]. However, this research does not assume environmental changes, and there is limited research on wheel-type snake robots traversing variable terrains.

Many disaster sites are discontinuous environments with scattered footholds. Hence, snake robots need to transfer from one environment to another to operate efficiently at disaster sites. In the prior research, control methods for snake robots to ascend and descend parallel steps were proposed [7], [8], [11], [18], [19]. Tanaka introduced a stair-climbing method for snake robots [21], whereas Nakajima presented a control method for snake robots to move between two non-parallel planes [10]. However, these approaches do not account for environmental changes. Since disaster sites have unstable footholds such as rubble, transfer motions must be adaptable to the changing environment.

Hence, we focus on discontinuous environments scattered with variable footings, such as those encountered at disaster sites. To realize movement in such an environment, this paper proposes a control method for a passive-wheeled snake robot to adapt to changes in the environment and move between two variable planes. To achieve this purpose, we propose a control method enabling the snake robot to adapt to environmental changes. The proposed method uses proximity sensors to estimate the distance and direction relative to the surrounding environment. In cases where the robot's wheels lose contact with the plane due to environmental changes, the system executes recovery controls to reestablish contact between the wheels and the plane. By combining sensor information with propulsion and recovery control, the snake robot can adapt to changes of the environment and traverse between two variable planes. The main contribution of the proposed method is that it can solve the problem of moving between two planes under variable footings, which has not been solved in previous studies on snake robots. We validate the effectiveness of the proposed method through experiments utilizing an actual robot.

II. PROBLEM SETTING

The robot used in this research is shown in Fig.1(a). This robot consists of $2n$ links and $2n - 1$ joints. It features alternating single-axis pitch and yaw joints. The length of

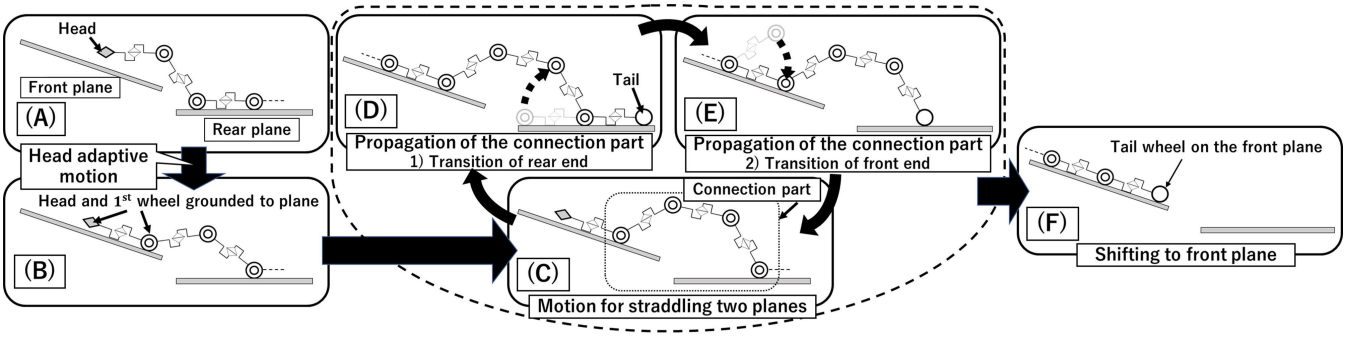

FIGURE 3. Flow of moving between two planes.

the link connecting adjacent joints is l. The joint connecting the ith link to the $i+1$th link is the ith joint. The relative angle between the ith and the $i+1$th link is ψ_i, is directly controlled by the ith joint. Let $\boldsymbol{\psi} \in \mathbb{R}^{2n-1,1}$ be a vector of all relative joint angles. Let $1, 3, \cdots, 2n-1$th joints be yaw joints and the $2, 4, \cdots, 2(n-1)$th joints be pitch joints. The robot has passive wheels with anisotropic friction, coaxial to the pitch joint. These wheels are slippery in the propulsive direction and less slippery in the orthogonal direction. Leveraging this anisotropy and rotating the joints, the snake robot can be propelled. This configuration is widely used in previous studies [2], [3], [7], [8], [10], and various behaviors can be achieved by applying the methods of previous studies. Additionally, the robot is equipped with a proximity sensor aligned with the wheel axis. As shown in Fig.1(b), this proximity sensor measures the minimum distance and direction angle in the radial direction of the sensor to the plane. Since the wheels rotate, the sensor on the ith wheel axle is fixed to the rear link of the ith wheel ($2i+1$th link), not to the wheel but to the link. So the orientation of the sensor changes in conjunction with the rear link as shown in Fig.1(c). This is a requirement for estimating the relative relationship between the robot and the environment based on the robot's geometric relationship and sensor information.

Fig.2(a) shows the assumed environment, comprising two unstable planes with variable inclinations. Fig.2(b) shows the names of each part of the robot. The section of the robot grounded on the front plane is referred to as the front plane part, whereas the part grounded on the rear plane is referred to as the rear plane part. The connection part is the segment connecting the rear-end wheels of the front plane to the front-end wheels of the rear plane. Fig.2(a) defines four relative coordinate systems for the robot: the head coordinate system Σ_h, the front-end of the connection part Σ_{cf}, the rear-end of the connection part Σ_{cr}, and the ith link coordinate system Σ_i.

Fig.3 shows the robot's motion flow in the assumed environment, based on Nakajima's method [10]. Initially, the robot head is grounded to the front plane by performing 'head adaptive motion' (A-B). Afterward, the robot performs 'motion for straddling two planes' (C) to move between the planes. Next, it performs the 'propagation of the connection part' (D-E), moving the connection part backward as it advances. By repeating the cycle from (C-E), the robot's entire body eventually reaches the front plane (F).

This paper focuses on the motion for straddling two planes among these motions. In this motion, the robot propels by utilizing the anisotropy friction of the wheels based on each plane. Furthermore, controlling the connection part joints ensures proper contact with the wheels on the plane [5]. Consequently, the ground contact of the wheels to the plane and the information such as the position and angle of each plane are necessary for the robot's propulsion. However, information of plane changes in the variable two-plane environment. Methods such as Nakajima's method [10], which provides predetermined information of plane, are not applicable in this study. Additionally, changes in the plane inclinations may cause the wheels on both planes to lose contact while propelling. The propulsion control in this study [5] assumes that all wheels on the front plane part and the rear plane part are grounded. However, when the wheels become ungrounded, the propulsion control behaves differently from the assumption. As a result, conventional methods fail to reestablish contact between an ungrounded wheel from the front plane part and the plane.

To address these problems, this paper proposes the motion for straddling two variable planes that improve the motion in Nakajima's method [10]. The motion for straddling two variable planes, as illustrated in Fig.4, executes two types of controls: propulsion control and recovery control. When all wheels of both plane parts are correctly grounded, the robot propels itself on the environment using propulsion control. The control estimates the distance and direction relative to the surrounding environment based on the information from the sensors. The controller controls the robot according to the robot's relative coordinate system based on this estimated information. When the sensor detects ungrounded wheels on either plane, the robot executes the recovery control to ground the wheel on the plane again. After the recovery control, the robot resumes propulsion control. This approach ensures that the robot adapts its wheels to

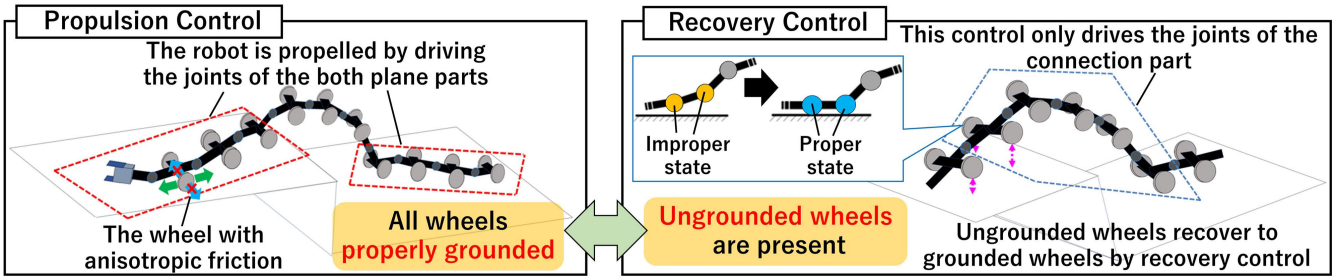

FIGURE 4. Overview of the proposed method.

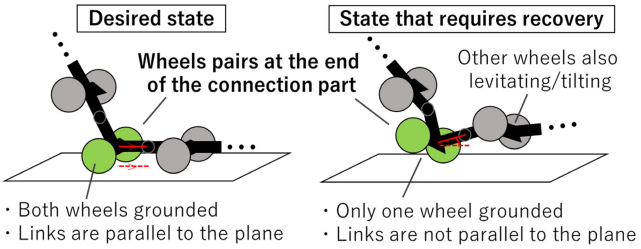

FIGURE 5. The posture that requires recovery control: The desired state entails wheel pairs at both ends of the connection part being grounded to the plane, with the links aligned parallel to the plane.

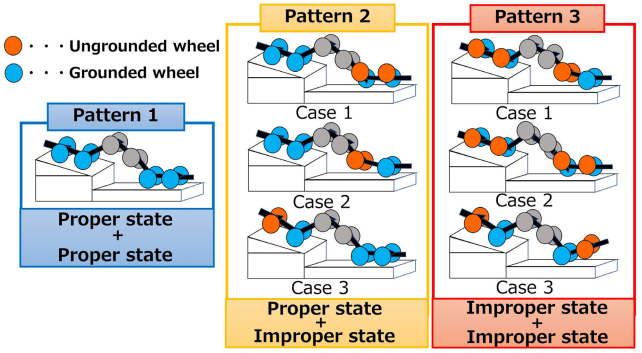

FIGURE 6. Classification of conditions requiring recovery control.

environmental changes and resumes propulsion, enabling the snake robot to traverse between two variable planes.

III. PROPOSED METHOD

A. RECOVERY CONTROL

Fig.5 shows the postures that require recovery control. As depicted, recovery control is started when the wheel pairs at either end of the connection part are ungrounded or when the links are not parallel to the plane. In the propulsion control, the pitch joint angles in both plane parts are fixed at 0 rad. Consequently, the grounding condition of the wheels of the connection part influences the remaining wheels on the plane part. If the wheel at the end of the connection part is properly grounded to the plane, all wheels on the plane achieve proper grounding. The recovery control uses one of the connection part's end wheels as a reference point to control the wheels on the other end of the connection part to the desired grounding state. In this case, the reference point is assumed fixed, while the connection joints control the motion of the control point.

Fig.6 shows the assumed state of the wheels at both ends of the connection part. The wheels on the both ends of the connection part can be either both wheels grounded, only one wheel grounded, or both ungrounded. The combination of those states can be grounded into 3 patterns. This paper proposes a control model that can recover from Pattern 2.

The reference coordinate system in the recovery control is defined as Σ_{rec}. Σ_{rec} takes either Σ_{cf} or Σ_{cr} in Fig.2(a) which the wheels are properly grounded. The grounding state of each wheel is determined from sensor information.

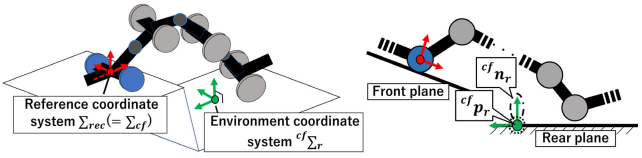

FIGURE 7. Coordinate system used to estimate information of plane.

1) ESTIMATION OF INFORMATION OF PLANE

When Σ_{rec} is set to Σ_{cf}, we define ${}^{cf}\boldsymbol{p}_r \in \mathbb{R}^{3,1}$ as the coordinates of a point on the rear plane from Σ_{cf} and ${}^{cf}\boldsymbol{n}_r \in \mathbb{R}^{3,1}$ as the normal vector of the rear plane from Σ_{cf} as the information of plane to be used. To estimate this information of plane, the proposed method calculates the rear plane coordinate system ${}^{cf}\Sigma_r$ observed from Σ_{cf} shown in Fig.7. This coordinate system's origin is anchored on the plane, with arbitrarily oriented x- and y-axes, and the z-axis oriented perpendicular to the plane.

${}^{cf}\Sigma_r$ is calculated from sensor information. Table 1 and Fig.8 show the parameters used to estimate information of plane. The wheel at the front-end of the connection part is defined as n_{fe}th wheel, whereas the wheel at the rear-end is defined as the n_{re}th wheel. The information of plane is derived from sensor data at both ends of the connection part, the distance from the axle center to the sensor a_s, the robot's link length l, and the joint angles of the connection part. The connection part has j_c number of joints, ranging from the $2n_{fe}$ joint to the $2n_{re}$ joint, encapsulated in the vector $\boldsymbol{\psi}_c \in \mathbb{R}^{j_c,1}$.

TABLE 1. Parameters used to estimate information of plane.

Variable	Variable's information
a_s	The distance from the axle center to the sensor
${}^{s}d_{l,i}$	Sensor distance information obtained from the ith left wheel
${}^{s}\phi_{l,i}$	Sensor direction information obtained from the ith left wheel
${}^{s}d_{r,i}$	Sensor distance information obtained from the ith right wheel
${}^{s}\phi_{r,i}$	Sensor direction information obtained from the ith right wheel

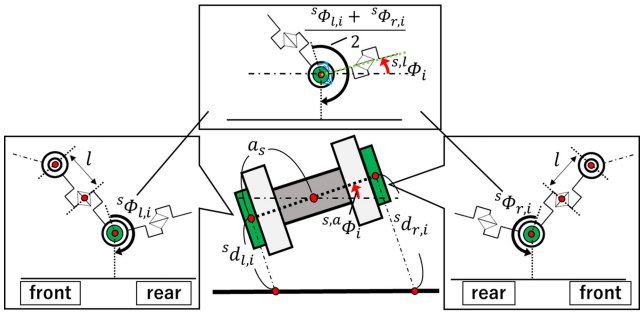

FIGURE 8. Illustration of parameters used to estimate information of plane.

${}^{s,l}\phi_i$ is the relative angle of the rear link of the i-th wheel to the plane, whereas ${}^{s,a}\phi_i$ is the roll axis relative angle of the ith wheel to the plane. These parameters are determined from sensor information ${}^{s}d_{l,i}$, ${}^{s}d_{r,i}$, ${}^{s}\phi_{l,i}$, and ${}^{s}\phi_{r,i}$ as

$$ {}^{s,l}\phi_i = \frac{{}^{s}\phi_{l,i} + {}^{s}\phi_{r,i}}{2} - \pi \tag{1} $$

$$ {}^{s,a}\phi_i = \tan^{-1}\left(\frac{{}^{s}d_{l,i} - {}^{s}d_{r,i}}{2a_s}\right). \tag{2} $$

The calculation of ${}^{s,l}\phi_i$ involves averaging the angle information obtained from both left and right sensors, mitigating errors inherent in individual sensors.

As shown in Fig.9, ${}^{cf}\Sigma_r$ is derived by a coordinate transformation based on a geometric relationship using l, $\boldsymbol{\psi}_c$, ${}^{s,l}\phi_{n_{re}}$, ${}^{s}d_{l,n_{re}}$, and ${}^{s,a}\phi_{n_{re}}$. ${}^{cf}\boldsymbol{p}_r$ is the coordinate origin of ${}^{cf}\Sigma_r$, and ${}^{cf}\boldsymbol{n}_r$ is the unit vector in the z-axis direction of ${}^{cf}\Sigma_r$.

Conversely, when Σ_{rec} is configured as Σ_{cr}, we define ${}^{cr}\boldsymbol{p}_f \in \mathbb{R}^{3,1}$ the coordinates of a point on the front plane observed from Σ_{cr}, and ${}^{cr}\boldsymbol{n}_f \in \mathbb{R}^{3,1}$ the normal vector of the front plane observed from Σ_{cr}, as the information of plane. This information is obtained from the front plane coordinate system ${}^{cr}\Sigma_f$ observed from Σ_{cr}.

2) CONTROL MODEL OF RECOVERY CONTROL

This section shows the control model of recovery control. In recovery control, only the connection part is subject to control. The control variables for the recovery control are shown in Fig.10. When Σ_{rec} is set to Σ_{cf}, the control object becomes the n_{re} wheel, which is the rear-end of the connection part. In this case, the control variables are the distance from the center of the left/right wheel to the plane $(d_{l,n_{re}}, d_{r,n_{re}})$, the relative angle between the rear link and the plane at the rear-end of the connection part (${}^{l}\phi_{n_{re}}$), and the 1st joint of the connection part (${}^{c}\psi_1$). $d_{l,n_{re}}$, $d_{r,n_{re}}$, and ${}^{l}\phi_{n_{re}}$ are obtained from

$$ d_{l,n_{re}} = {}^{cf}\boldsymbol{n}_r \cdot \left({}^{cf}\boldsymbol{p}_{l,n_{re}} - {}^{cf}\boldsymbol{p}_r\right), \tag{3} $$

$$ d_{r,n_{re}} = {}^{cf}\boldsymbol{n}_r \cdot \left({}^{cf}\boldsymbol{p}_{r,n_{re}} - {}^{cf}\boldsymbol{p}_r\right), \tag{4} $$

$$ {}^{l}\phi_{n_{re}} = \sin^{-1}\left({}^{cf}\boldsymbol{n}_r \cdot {}^{cf}\boldsymbol{l}_{2n_{re}+1}\right), \tag{5} $$

where ${}^{cf}\boldsymbol{p}_{l,n_{re}} \in \mathbb{R}^{3,1}$ and ${}^{cf}\boldsymbol{p}_{r,n_{re}} \in \mathbb{R}^{3,1}$ are the positions of the n_{re} left and right wheel center observed from Σ_{cf}, and ${}^{cf}\boldsymbol{l}_{2n_{re}+1} \in \mathbb{R}^{3,1}$ is the direction vector of the $2n_{re}+1$th link observed from Σ_{cf}. These values are computed based on $\boldsymbol{\psi}_c$. To properly ground the wheel pairs at both ends of the connection part to the plane, the targets for $d_{l,n_{re}}$ and $d_{r,n_{re}}$ are set to the wheel radius r_w, whereas the target for ${}^{l}\phi_{n_{re}}$ is set to 0.

Conversely, when Σ_{rec} is set to Σ_{cr}, the control object shifts the n_{re}th wheel, located at the front-end of the connection part. In this case, the defined control variables encompass $d_{l,n_{fe}}$, $d_{r,n_{fe}}$, ${}^{-l}\phi_{n_{fe}}$, and ${}^{c}\psi_1$. ${}^{-l}\phi_{n_{fe}}$ and ${}^{-l}\phi_{n_{fe}}$ is the relative angle of the front link of the front-end wheel of the connection part to the plane, as shown in Fig.10. These values are obtained as

$$ d_{l,n_{fe}} = {}^{cr}\boldsymbol{n}_f \cdot \left({}^{cr}\boldsymbol{p}_{l,n_{re}} - {}^{cr}\boldsymbol{p}_f\right), \tag{6} $$

$$ d_{r,n_{fe}} = {}^{cr}\boldsymbol{n}_f \cdot \left({}^{cr}\boldsymbol{p}_{r,n_{fe}} - {}^{cr}\boldsymbol{p}_f\right), \tag{7} $$

$$ {}^{-l}\phi_{n_{fe}} = \sin^{-1}\left({}^{cr}\boldsymbol{n}_\sigma \cdot (-{}^{cr}\boldsymbol{l}_{2n_{fe}})\right). \tag{8} $$

The variables used in these equations share fundamental definitions with those in (3)-(5), although with the reference coordinate system designated as Σ_{cr}. These control variables are similarly derived from $\boldsymbol{\psi}_c$, with the targets of $d_{l,n_{fe}}$, $d_{r,n_{fe}}$ being r_w and ${}^{-l}\phi_{n_{fe}}$ being 0.

The control variable ${}^{c}\psi_1$ serves the purpose of accommodating sensor errors. The output characteristics of the sensor are shown in Fig.11. In Fig.11(a), the sensor's error amount fluctuates according to the distance and orientation relative to the object under observation. The maximum error in distance information approximates 6 mm, whereas the maximum error in directional information reaches around 0.6 rad. As shown in Fig.11, the sensor has a certain level of error, contingent upon its distance and orientation relative to the detected object. Furthermore, even when maintaining specific distance and orientation parameters, the sensor output fluctuates within a certain range.

Recovery control are planned to be terminated when the control variable converges to the target value. Notably, when encountering substantial sensor errors, a certain deviation between the control variable and the target may persist, as illustrated in Fig.12(a). Under such circumstances, the recovery control may not end. To prevent this problem, it needs to minimize sensor errors by compensating for sensor values. As shown in Fig.11(b), the sensor has a characteristic where the error value changes according to the distance and the orientation relative to the object. However, setting correction values for all conditions within the sensor's

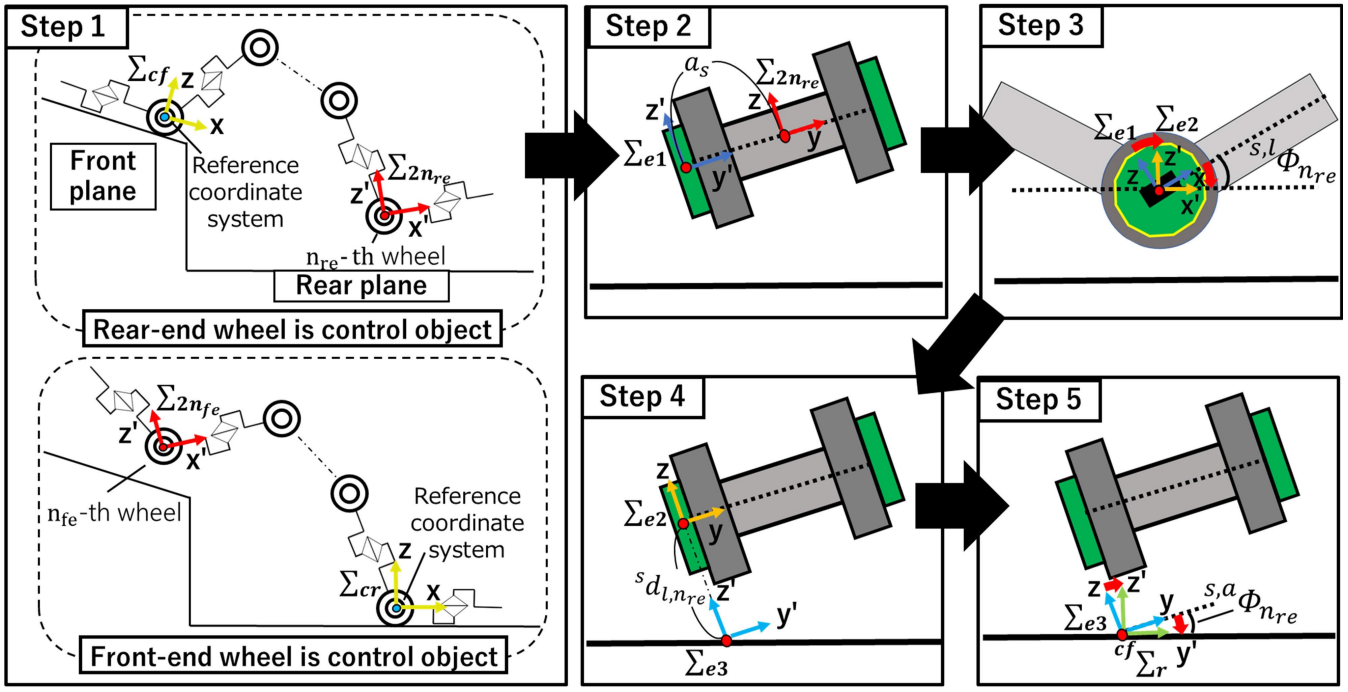

FIGURE 9. Procedure for calculating information of plane : Transform from the reference coordinate system Σ_{cf} to Σ_{2nre} (Step 1). Next, Σ_{2nre} is translated by $-a_s$ in the direction of y axis (Step 2). After that, rotate the transformed coordinate system Σ_{e1} by ${}^{s,l}\phi_{nre}$ in y-axis direction (Step 3). Then, translate the transformed coordinate system Σ_{e2} by $-{}^{s}d_{l,nre}$ in the direction of z axis (Step 4). Finally, rotate the transformed coordinate system Σ_{e3} by ${}^{s,a}\phi_{nre}$ along x axis (Step 5). These steps finally yield the coordinate system ${}^{cf}\Sigma_r$. In the case of deriving ${}^{cr}\Sigma_f$, the difference is that the coordinate transformation from Σ_{cr} to Σ_{2nfe} in step 1, and the variables used in steps 2 to 5 being ${}^{s,l}\phi_{nfe}$, ${}^{s}d_{l,nfe}$, and ${}^{s,a}\phi_{nfe}$.

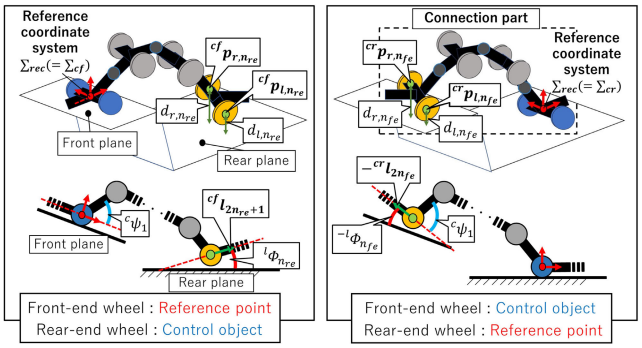

FIGURE 10. Control variables in recovery control.

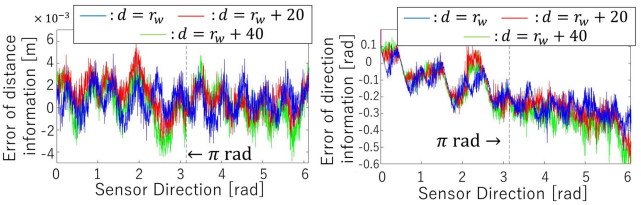

(a) Output characteristics for every sensor orientation : The figure shows the output characteristics when the distance from the object is r_w mm, $r_w + 20$ mm, and $r_w + 40$ mm.

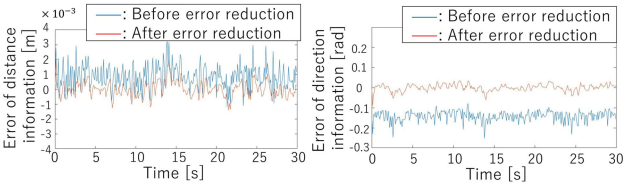

(b) Output characteristics of the sensor at a fixed distance and orientation : The figure shows the output characteristics when the distance to the object is r_w mm and the orientation of the sensor is π rad. The figure also shows the results before and after the sensor error was reduced by offset and filtering.

FIGURE 11. Output characteristics of the sensor.

measurement range of the sensor is difficult. Consequently, we use a sensor that specifically reduces errors within the measurement area relevant to the recovery control. To achieve this, we first establish the target posture for the recovery control, which is the desired state for both ends of the connection part as shown in Fig.5, and let the robot take the posture. The value of ${}^{c}\psi_1$ when the robot is assumed in this posture is ${}^{c}\psi_{1,adv}$, and the extracted sensor values are ${}^{s}d_{adv}$ and ${}^{s}\phi_{adv}$.

Then, as shown in Fig.12(b), the difference $(\varepsilon_d, \varepsilon_\phi)$ from the ideal value $({}^{s}d_d, {}^{s}\phi_d)$ is used as the offset value. In the experiment, values obtained from the sensors undergo a moving average filter, and the values added to ε_d and ε_ϕ are utilized to estimate information of plane. As the result, as shown in Fig.11(b), the distance information's error is diminished to under 2 mm, and the direction information's error is diminished to under 0.1 rad.

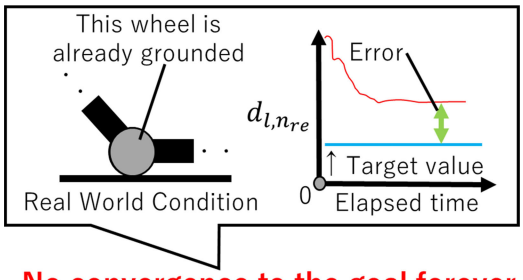

No convergence to the goal forever

(a) Problems caused by sensor errors in recovery control

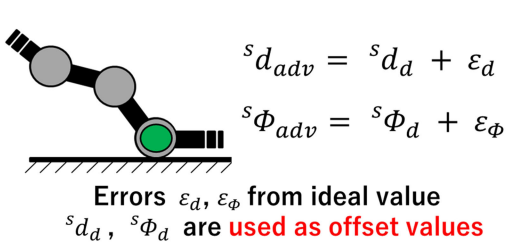

(b) Reduction of sensor information error due to offset

FIGURE 12. Problems caused by sensor errors and their countermeasures.

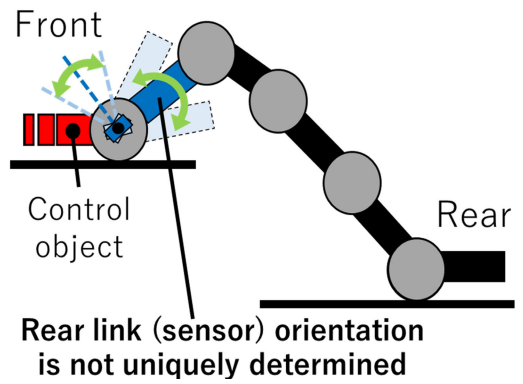

FIGURE 13. Problems on the front-end of the connection part that occur when ${}^{c}\psi_{1}$ is not controlled.

To prevent sensor errors after offsetting, the sensor must maintain the same position and orientation relative to the plane as when ${}^{s}d_{adv}$ and ${}^{s}\phi_{adv}$ were acquired. The final positional relationship between the sensor and the plane will match the state when ${}^{s}d_{adv}$ and ${}^{s}\phi_{adv}$ were acquired by controlling $d_{l,n_{fe}}$, $d_{r,n_{fe}}$, $d_{l,n_{re}}$, and $d_{r,n_{re}}$. As shown in Fig.1(c), the sensor's orientation changes along with the rear link. When executing recovery control at the rear-end of the connection part, the final orientation of the rear link (sensor) aligns with the orientation when ${}^{s}d_{adv}$ and ${}^{s}\phi_{adv}$ were acquired by controlling ${}^{l}\phi_{n_{re}}$. Consequently, the recovery control at the rear-end can reduce sensor errors within the utilized measurement area. However, as shown in Fig.13, when executing the recovery control of the front-end of the connection part, simply controlling ${}^{-l}\phi_{n_{fe}}$ cannot guarantee that the final rear link orientation matches the one when ${}^{s}d_{adv}$ and ${}^{s}\phi_{adv}$ are acquired. So the appropriate offset value cannot be estimated due to the sensor's characteristic of error variation with orientation.

Thus, as shown in Fig.14, we control ${}^{c}\psi_{1}$ so that the sensor direction always matches the direction when ${}^{s}d_{adv}$ and ${}^{s}\phi_{adv}$ are acquired. The corresponding target value is determined by

$$ {}^{c}\psi_{1,d} = {}^{c}\psi_{1,adv} + {}^{s,-l}\phi_{n_{fe}}. \tag{9} $$

Fig.15 shows ${}^{s,-l}\phi_{n_{fe}}$ as the relative angle between the front link of the n_{fe}th wheel and the plane, calculated from sensor information and obtained by

$$ {}^{s,-l}\phi_{n_{fe}} = {}^{s,l}\phi_{n_{fe}} - \psi_{2n_{fe}}, \tag{10} $$

where let $\psi_{2n_{fe}}$ be the $2n_{fe}$th element of $\boldsymbol{\psi}$. The value of ${}^{c}\psi_{1,adv}$ is set as $-\pi/6$.

A velocity constraint in lateral direction of the controlled wheel is generated when it is grounded on the plane. Therefore, when the reference coordinate system is Σ_{cf}, the velocity constraint equation for the wheel is expressed as

$$ {}^{cf}x_{n_{re}} \sin {}^{cf}\theta_{n_{re}} - {}^{cf}y_{n_{re}} \cos {}^{cf}\theta_{n_{re}} = 0, \tag{11} $$

where ${}^{cf}x_{n_{re}}$, ${}^{cf}y_{n_{re}}$, and ${}^{cf}\theta_{n_{re}}$ are the projected position and orientation of the velocity constraint point of the rear-end wheel of the connection part, as shown in Fig.16(a). The constraint point can be either the axle center, the point nearest to the plane in the wheel pair, or no constraint, as shown in Fig.16(b). The choice of the constraint point depends on the distance between the estimated plane and the left and right wheels. Similarly, when the reference coordinate system is Σ_{cr}, the velocity constraint was applied to the front-end wheel.

The time-differentiated equations for the control variables and (11) can be summarized for $\boldsymbol{\psi}_{c}$ as

$$ \dot{\boldsymbol{r}} = \boldsymbol{J}\dot{\boldsymbol{\psi}}_{c}, \tag{12} $$

$$ \boldsymbol{D}\dot{\boldsymbol{\psi}}_{c} = 0. \tag{13} $$

where $\boldsymbol{J} = \partial \boldsymbol{r}/\partial \boldsymbol{\psi}_{c} \in \mathbb{R}^{4,j_c}$, $\boldsymbol{D} \in \mathbb{R}^{1,j_c}$. $\boldsymbol{r}$ denotes the grouping of control variables, expressed as $\boldsymbol{r} = [d_{l,n_{re}}, d_{r,n_{re}}, {}^{l}\phi_{n_{re}}, {}^{c}\psi_{1}]^{\top}$. Summarizing (12) and (13) yields a kinematic model of recovery control as

$$ \begin{bmatrix} \dot{\boldsymbol{r}} \\ 0 \end{bmatrix} = \boldsymbol{H}\dot{\boldsymbol{\psi}}_{c}, \tag{14} $$

where $\boldsymbol{H} = [\boldsymbol{J}^{\top}, \boldsymbol{D}\top]^{\top} \in \mathbb{R}^{5,j_c}$.

3) CONTROL INPUT OF RECOVERY CONTROL

The target values of the controlled variable for the kinematic model in (14) are summarized in the vector $r_{d} = [r_{w}, r_{w}, 0, -\pi/6 + {}^{s,-l}\phi_{n_{fe}}]^{\top}$. The control input, which is angular velocity $\dot{\boldsymbol{\psi}}_{c}$ of each joint of the connection part, can be calculated by

$$ \dot{\boldsymbol{\psi}}_{c} = \boldsymbol{H}^{\dagger} \begin{bmatrix} \dot{\boldsymbol{r}}_{d} + \boldsymbol{K}_{r}(\boldsymbol{r}_{d} - \boldsymbol{r}) \\ 0 \end{bmatrix} + k_{r}(\boldsymbol{I} - \boldsymbol{H}^{\dagger}\boldsymbol{H})\boldsymbol{\eta}^{\top}, \tag{15} $$

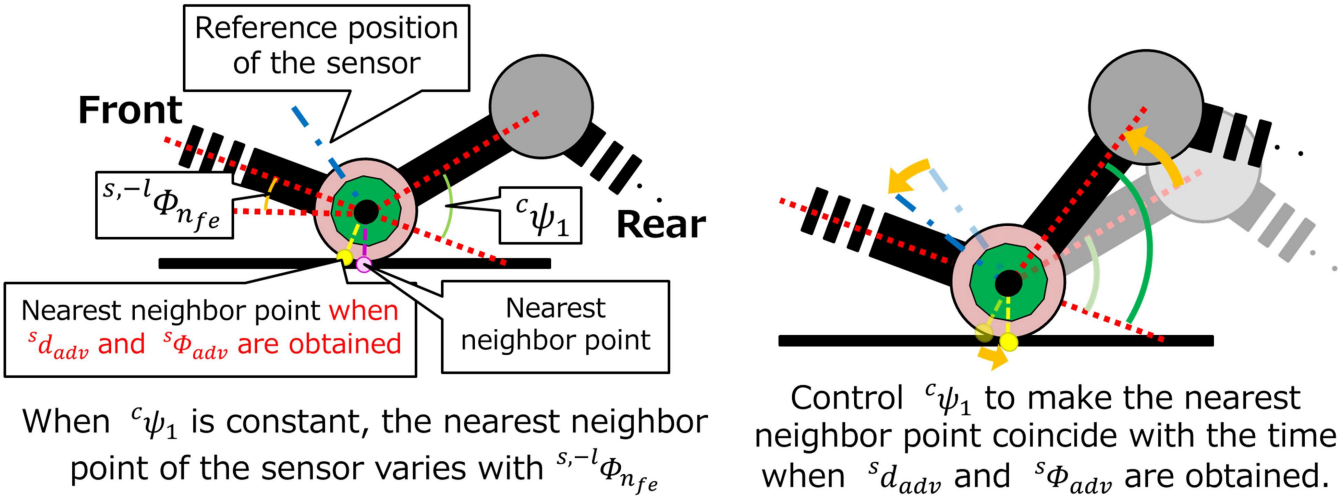

FIGURE 14. Control of ${}^{c}\psi_1$.

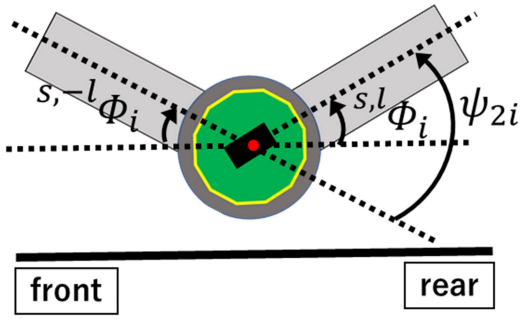

FIGURE 15. Variable ${}^{s,-l}\phi_i$ Definition.

where, $\boldsymbol{H}^{\dagger}$ is the pseudo-inverse of $\boldsymbol{H}$, $\boldsymbol{K}_r \in \mathbb{R}^{4,4}$ consists of positive constant gains in its diagonal components, k_r is a gain regarding redundancy, and $\boldsymbol{\eta} \in \mathbb{R}^{j_c,1}$ is an arbitrary row vector. Substituting (15) into (14) yields

$$\dot{\boldsymbol{r}}_d - \dot{\boldsymbol{r}} + \boldsymbol{K}_r(\boldsymbol{r}_d - \boldsymbol{r}) = 0, \tag{16}$$

and the controlled variable $\boldsymbol{r}$ converges to the target value $\boldsymbol{r_d}$ at $t \to \infty$.

The second term on the right side of (10) corresponds to the redundancy component. This term can contribute to accomplishing subtasks using redundancy by defining an appropriate vector for $\boldsymbol{\eta}$. In recovery control, the subtasks are to avoid the limits of movement of the connection part joints and to prevent contact of the connection part with the environmental plane. The evaluation function V is obtained from

$$V = g_1 V_1 + g_2 V_2. \tag{17}$$

g_1 and g_2 are the weight coefficients for each function. V_1 is a function for avoiding joint motion limits, whereas V_2 is a function for preventing plane contact of the connection part. These functions are calculated as

$$V_1 = \frac{1}{j_c}\sum_{i=1}^{j_c}\frac{\psi_{lim}^2 - {}^{c}\psi_i^2}{\psi_{lim}^2}, \tag{18}$$

$$V_2 = \frac{1}{m_c - 2}\sum_{i=2}^{m_c-1}\frac{d_{h1}^2 - (d_{c,i} - d_{h2})^2}{d_{h1}^2}, \tag{19}$$

where, ψ_{lim} is the limit angle of joint motion, ${}^{c}\psi_i$ is the ith component of $\boldsymbol{\psi}_c$, j_c is the number of joints in the connection part, m_c is the number of wheels in the connection part, $d_{c,i}$ is the distance from the ith wheel of the connection part to the plane, and d_{h1}, d_{h2} are arbitrary constants. When determining $d_{c,i}$, we calculate the distance from the ith wheel of the connection part to the front and rear plane, and the closer between those two is selected as $d_{c,i}$. The evaluation function is calculated from $\boldsymbol{\psi}_c$. The time-differentiated equation is given by

$$\dot{V} = \frac{\partial V}{\partial \boldsymbol{\psi}_c}\dot{\boldsymbol{\psi}}_c. \tag{20}$$

$\boldsymbol{\eta}$ in (15) is determined by

$$\boldsymbol{\eta} = \frac{\partial V}{\partial \boldsymbol{\psi}_c}. \tag{21}$$

Substituting the inputs to (15) into (20) yields

$$\dot{V} = \boldsymbol{\eta}\boldsymbol{H}^{\dagger}\cdot(\dot{\boldsymbol{r}}_d + \boldsymbol{K}_r(\boldsymbol{r}_d - \boldsymbol{r})) + k_v\boldsymbol{\eta}(\boldsymbol{I} - \boldsymbol{H}^{\dagger}\boldsymbol{H})\boldsymbol{\eta}^{\top}. \tag{22}$$

The first term on the right side of this equation represents the component that depends on the control variable at the connection part. The second term on the right side is always non-negative when k_r is a positive constant gain. Consequently, the component independent of the controlled variable can contribute to increasing $\dot{V}$, thereby achieving the subtasks.

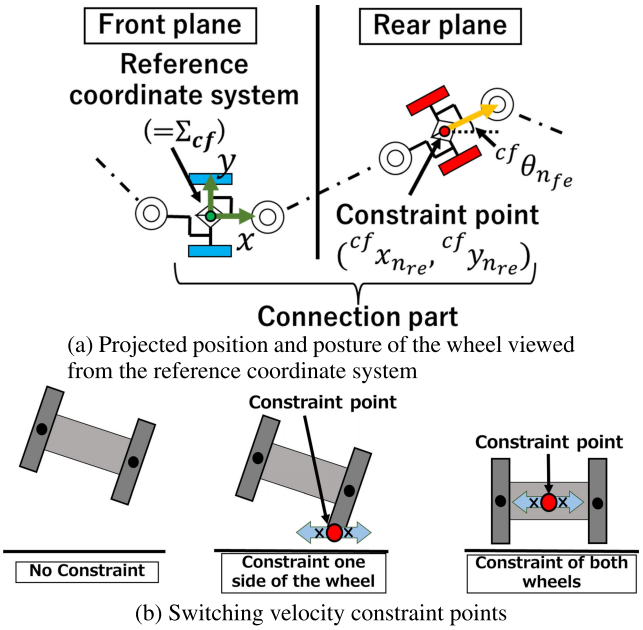

FIGURE 16. Velocity constraint of the wheel to be controlled.

B. PROPULSION CONTROL

As shown in Fig.4, the proposed method propels the robot using propulsion control except when ungrounded wheels occur. The proposed propulsion control is based on the motion for straddling two planes proposed in Nakajima's method [10]. As described in Section II, the propulsion control propels the robot by rotating the joints of the plane part. Additionally, the connection part joints are controlled to maintain proper contact with the wheels of the plane part during propulsion. To enable this motion, the control model for propulsion control comprises two models: a two-dimensional model for the plane part and a three-dimensional model for the connection part. Separating the models prevents excessive complexity in the control model due to the three-dimensional control model of the plane part. Section III-B1 describes the model for maintaining wheel contact in the connection part. Section III-B2 describes the model for undulating motion in both plane parts.

1) CONTROL MODEL OF THE CONNECTION PART

In propulsion control, the connection part is responsible for maintaining the wheels of the plane part grounded. This motion involves maintaining contact with the rear-end wheel of the connection part while assuming that the wheel of the front plane part is grounded. The control variable in this motion is $d_{l,n_{re}}$, $d_{r,n_{re}}$, ${}^{l}\phi_{n_{re}}$, and ${}^{c}\psi_1$. In the calculation of the control variables, the reference coordinate system is set as the robot's head Σ_h, and ${}^{h}\boldsymbol{p}_r \in \mathbb{R}^{3,1}$, ${}^{h}\boldsymbol{n}_r \in \mathbb{R}^{3,1}$ obtained by the procedure in Fig.9 are used as information of plane. Fig.17 illustrates the propagation motion of the connection part in this method ((D-E) in Fig.3). This motion is based on the sensor information of the second wheel of the connection part. When the robot continues propulsion control, the second wheel of the connection part reaches above the front plane. At that time, the sensor mounted on this wheel detects the plane. And the robot can execute the propagation motion at the appropriate timing. Consequently, ${}^{c}\psi_1$ is included as a control variable to prevent excessive lifting of the second wheel and to recognize the front plane. The target value of ${}^{c}\psi_1$ during propulsive control is set to $-\pi/6$ rad similar to ${}^{c}\psi_{1,adv}$ in recovery control.

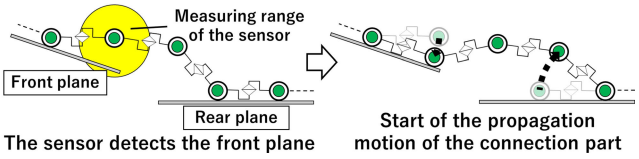

FIGURE 17. The propagation motion of the connection part.

The control model for the connection part is derived by combining the time derivative equation of the control variables and the velocity constraint equation of the wheel, similar to the recovery control, with only the reference coordinate system set on Σ_h.

Whereas the recovery control assumes the reference coordinate system as Σ_{cf} or Σ_{cr}, the propulsion control is based on the Σ_h. When Σ_h is the reference coordinate system, the position and posture of the front-end wheel of the connection part are obtained from the projected position and orientation of the robot head $\boldsymbol{w}=[x_h, y_h, \theta_h]^\top$ and the yaw joint angle of the front plane part. Accordingly, the kinematic model is derived in the same way as (12)-(14), giving

$$\begin{bmatrix} \dot{\tilde{\boldsymbol{r}}} \\ 0 \end{bmatrix} = \begin{bmatrix} \boldsymbol{H}_1 \ \boldsymbol{H}_2 \ \boldsymbol{H}_3 \end{bmatrix} \begin{bmatrix} \dot{\boldsymbol{w}}_h \\ \dot{\boldsymbol{\psi}}_{f,z} \\ \dot{\boldsymbol{\psi}}_c \end{bmatrix}, \tag{23}$$

where $\boldsymbol{H}_1 \in \mathbb{R}^{5,3}$, $\boldsymbol{H}_2 \in \mathbb{R}^{5,n_{fe}}$, and $\boldsymbol{H}_3 \in \mathbb{R}^{5,j_c}$. $\dot{\tilde{\boldsymbol{r}}} \in \mathbb{R}^{4,1}$ is a vector grouping the four control variables, and $\dot{\boldsymbol{\psi}}_{f,z} \in \mathbb{R}^{n_{fe},1}$ is a vector grouping the yaw joint angles of the front plane part. In the recovery control, the velocity constraint equation for the rear-end of the connection part determines the constraint target based on the positional relationship between its wheel and the rear plane. However, in propulsion control, the wheels are already sufficiently close to the plane by the recovery control. Thus, the velocity constraint point is always on the axle center.

2) CONTROL MODEL OF BOTH PLANE PARTS

In propulsion control, the plane part performs arbitrary trajectory tracking control of the robot head. Undulation motions are performed in the front and rear plane parts, referencing the head coordinate system Σ_h. This control model assumes that the wheels in each plane part are properly grounded by the control of the connection part. Consequently,

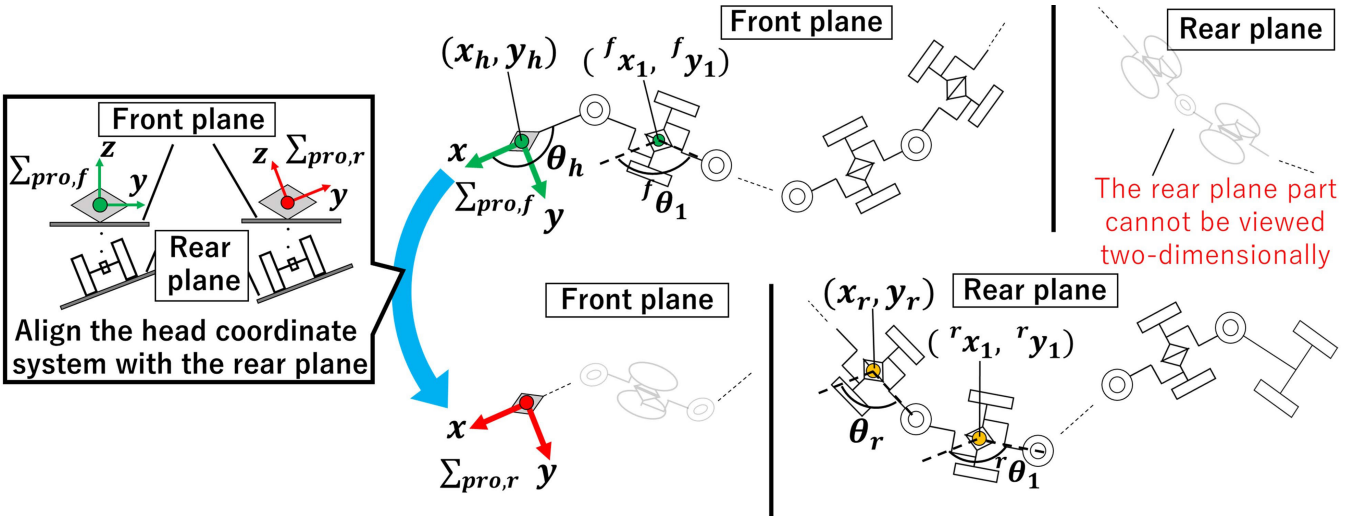

FIGURE 18. Velocity constraints of the plane part wheels.

the wheel velocity constraint equation can be expressed as

$$\begin{cases} {}^{f}\dot{x}_i \sin {}^{f}\theta_i - {}^{f}\dot{y}_i \cos {}^{f}\theta_i = 0, \\ {}^{r}\dot{x}_i \sin {}^{r}\theta_i - {}^{r}\dot{y}_i \cos {}^{r}\theta_i = 0. \end{cases} \tag{24}$$

${}^{f}x_i$, ${}^{f}y_i$, and ${}^{f}\theta_i$ represent the position and orientation of the ith wheel in the front plane part relative to the reference coordinate system, whereas ${}^{r}x_i$, ${}^{r}y_i$, and ${}^{r}\theta_i$ represent the position and orientation of the ith wheel in the rear plane part relative to the reference coordinate system. Fig.18 shows the projected position and orientation of the wheels in each plane part. In this figure, $\Sigma_{pro,f}$ is defined as Σ_h, and $\Sigma_{pro,r}$ as the coordinate system in which Σ_h is rotated to match the attitude of the rear plane. ${}^{f}x_i$, ${}^{f}y_i$, and ${}^{f}\theta_i$ are calculated based on $\Sigma_{pro,f}$ and ${}^{r}x_i$, ${}^{r}y_i$, and ${}^{r}\theta_i$ are calculated based on $\Sigma_{pro,r}$. To obtain $\Sigma_{pro,r}$, information of the 3D orientation of the rear plane relative to Σ_h is necessary and can be calculated based on sensor information. Since the first wheel of the rear plane part can be assumed to be grounded due to the control of the connection part, the velocity constraint equation for the rear plane part covers the wheels beyond the second wheel.

${}^{f}x_i$, ${}^{f}y_i$, and ${}^{f}\theta_i$ are calculated from $\boldsymbol{w}_h$ and $\boldsymbol{\psi}_{f,z}$, whereas ${}^{r}x_i$, ${}^{r}y_i$, and ${}^{r}\theta_i$ are calculated from the projected position and orientation $\boldsymbol{w}_r$=$[x_r, y_r, \theta_r]^{\mathrm{T}}$ of the rear-end of the connection part and the yaw joint angle $\boldsymbol{\psi}_{r,z} \in \mathbb{R}^{n-n_{re},1}$ of the rear plane part. Given that the proposed method is based on Σ_h, the actual value of $\boldsymbol{w}_h$ is always $[0, 0, \pi]^{\top}$.

Summarizing (24) in terms of $\boldsymbol{w}_h$, $\boldsymbol{\psi}_{f,z}$, $\boldsymbol{w}_r$, and $\boldsymbol{\psi}_{r,z}$, we obtain

$$\boldsymbol{A}_1 \dot{\boldsymbol{w}}_h = \boldsymbol{B}_1 \dot{\boldsymbol{\psi}}_{f,z}, \tag{25}$$

$$\boldsymbol{A}_2 \dot{\boldsymbol{w}}_r = \boldsymbol{B}_2 \dot{\boldsymbol{\psi}}_{r,z}. \tag{26}$$

To represent the motion of both plane parts as a unified control model, (26) needs to be expressed as an equation summarized by $\boldsymbol{w}_h$. From the geometric relationship of the robot, $\boldsymbol{w}_r$ can use $\boldsymbol{w}_h$, $\boldsymbol{\psi}_{f,z}$, and $\boldsymbol{\psi}_c$ to express

$$\dot{\boldsymbol{w}}_r = \boldsymbol{J}_{r,1} \dot{\boldsymbol{w}}_h + \boldsymbol{J}_{r,2} \dot{\boldsymbol{\psi}}_{f,z} + \boldsymbol{J}_{r,3} \dot{\boldsymbol{\psi}}_c. \tag{27}$$

The position and orientation of the rear plane relative to Σ_h change over time because the plane of the assumed environment changes. Therefore, it is originally necessary to include a term in (27) to account for the time variation of the information of plane in the rear plane. However, if the plane changes, it is judged that the wheels lose proper ground contact, and propulsion is resumed after the ungrounded wheels are properly grounded using the recovery control. Consequently, the information of plane in the rear plane is assumed to be invariant in the propulsion control model. This assumption allows $\dot{\boldsymbol{w}}_r$ to be expressed without considering the time variation of the information of plane in the rear plane. Substituting (27) into (26) yields

$$\boldsymbol{A}_2 \boldsymbol{J}_{r,1} \dot{\boldsymbol{w}}_h = \begin{bmatrix} -\boldsymbol{A}_2 \boldsymbol{J}_{r,2} & -\boldsymbol{A}_2 \boldsymbol{J}_{r,3} & \boldsymbol{B}_2 \end{bmatrix} \begin{bmatrix} \dot{\boldsymbol{\psi}}_{f,z} \\ \dot{\boldsymbol{\psi}}_c \\ \dot{\boldsymbol{\psi}}_{r,z} \end{bmatrix}. \tag{28}$$

By summarizing (25) and (28), the control model for both plane parts is obtained as

$$\tilde{\boldsymbol{A}} \dot{\boldsymbol{w}}_h = \tilde{\boldsymbol{B}} \begin{bmatrix} \dot{\boldsymbol{\psi}}_{f,z} \\ \dot{\boldsymbol{\psi}}_c \\ \dot{\boldsymbol{\psi}}_{r,z} \end{bmatrix}, \tag{29}$$

$$\tilde{\boldsymbol{A}} = \begin{bmatrix} \boldsymbol{A}_1 \\ \boldsymbol{A}_2 \boldsymbol{J}_{r,1} \end{bmatrix}, \tag{30}$$

$$\tilde{\boldsymbol{B}} = \begin{bmatrix} \boldsymbol{B}_1 & \boldsymbol{0} & \boldsymbol{0} \\ -\boldsymbol{A}_2 \boldsymbol{J}_{r,2} & -\boldsymbol{A}_2 \boldsymbol{J}_{r,3} & \boldsymbol{B}_2 \end{bmatrix}, \tag{31}$$

where $\tilde{\boldsymbol{A}} \in \mathbb{R}^{n+n_{fe}-n_{re},3}$, $\tilde{\boldsymbol{B}} \in \mathbb{R}^{n+n_{fe}-n_{re},n+n_{fe}-n_{re}+j_c}$.

3) CONTROL INPUT OF PROPULSION CONTROL

In these kinematic models (23) and (29), the control input is calculated as the joint angular velocity from

$$\dot{\boldsymbol{\psi}}_{f,z} = \boldsymbol{B}_1^{-1}\boldsymbol{A}_1\dot{\boldsymbol{w}}_d, \tag{32}$$

$$\dot{\boldsymbol{\psi}}_c = \boldsymbol{H}_3^{\dagger}\left(\begin{bmatrix}\dot{\tilde{\boldsymbol{r}}}_d + \boldsymbol{K}_p(\tilde{\boldsymbol{r}}_d - \tilde{\boldsymbol{r}}) \\ 0\end{bmatrix} - \boldsymbol{H}_1\dot{\boldsymbol{w}}_d - \boldsymbol{H}_2\dot{\boldsymbol{\psi}}_{f,z}\right) + k_p(\boldsymbol{I} - \boldsymbol{H}_3^{\dagger}\boldsymbol{H}_3)\boldsymbol{\eta}^{\top}, \tag{33}$$

$$\dot{\boldsymbol{\psi}}_{r,z} = \boldsymbol{B}_2^{-1}\boldsymbol{A}_2\boldsymbol{J}_{r,1}\dot{\boldsymbol{w}}_d + \boldsymbol{B}_2^{-1}\left[\boldsymbol{A}_2\boldsymbol{J}_{r,2}\ \boldsymbol{A}_2\boldsymbol{J}_{r,3}\right]\begin{bmatrix}\dot{\boldsymbol{\psi}}_{f,z} \\ \dot{\boldsymbol{\psi}}_c\end{bmatrix}. \tag{34}$$

$\dot{\boldsymbol{w}}_d$ is the target relative velocity of the robot head, and $\tilde{\boldsymbol{r}}_d$ is the target value of $\tilde{\boldsymbol{r}}$. By substituting (32) and (34) into (29) yields

$$\tilde{\boldsymbol{A}}(\dot{\boldsymbol{w}}_d - \dot{\boldsymbol{w}}_h) = 0, \tag{35}$$

and if $\tilde{\boldsymbol{A}}$ is full rank, $\dot{\boldsymbol{w}}_h = \dot{\boldsymbol{w}}_d$. Substituting (33) into (23) gives

$$\dot{\tilde{\boldsymbol{r}}}_d - \dot{\tilde{\boldsymbol{r}}} + \boldsymbol{K}_p(\tilde{\boldsymbol{r}}_d - \tilde{\boldsymbol{r}}) = 0, \tag{36}$$

the control variable $\tilde{\boldsymbol{r}}$ converges to the target $\tilde{\boldsymbol{r}}_d$ at $t \to \infty$. The connection part control has redundancy based on (33). Substituting a vector $\boldsymbol{\eta}$ similar to (21), can contribute to accomplishing the same subtask as the recovery control.

C. CONTROL SWITCHING REQUIREMENTS

The proposed method executes propulsion control when the grounding condition of the wheels on the plane is satisfied. The system executes recovery control when an ungrounded wheel arises. Hence, appropriate switching of the control is needed. This section establishes the start and end conditions for the recovery control.

We define the vector $\boldsymbol{S}_i$=$[{}^s d_{l,i}, {}^s d_{r,i}, {}^s\phi_{l,i}, {}^s\phi_{r,i}]^{\top} \in \mathbb{R}^{4,1}$, which groups the sensor information obtained from the *ith* wheel. To determine the start of recovery control, we utilize six values: ${}^s d_{l,n_{fe}}$, ${}^s d_{r,n_{fe}}$, ${}^s d_{l,n_{re}}$, ${}^s d_{r,n_{re}}$, ${}^{s,-l}\phi_{n_{fe}}$ and ${}^{s,l}\phi_{n_{re}}$, derived from the distance and direction information of $\boldsymbol{S}_{n_{fe}}$ and $\boldsymbol{S}_{n_{re}}$. We calculate the error between the ideal values and the actual values for six values. If the error in either value exceeds a certain threshold, the recovery control is started. The start requirement of the recovery control can be expressed by

$$\begin{cases} |{}^s d_{l,n_{fe}} - {}^g d_{l,n_{fe}}| \geqq {}^j d_{l,n_{fe}} \\ |{}^s d_{r,n_{fe}} - {}^g d_{r,n_{fe}}| \geqq {}^j d_{r,n_{fe}} \\ |{}^{s,-l}\phi_{n_{fe}} - {}^g\phi_{n_{fe}}| \geqq {}^j\phi_{n_{fe}} \\ |{}^s d_{l,n_{re}} - {}^g d_{l,n_{re}}| \geqq {}^j d_{l,n_{re}} \\ |{}^s d_{r,n_{re}} - {}^g d_{r,n_{re}}| \geqq {}^j d_{r,n_{re}} \\ |{}^{s,l}\phi_{n_{re}} - {}^g\phi_{n_{re}}| \geqq {}^j\phi_{n_{re}} \end{cases}. \tag{37}$$

If any one of the requirements in (37) is satisfied, the recovery control is started. The first term on the left side of (37) represents the actual values, the second term on the left side represents the ideal values for each variable, and the right side represents the threshold values corresponding to the errors for each variable. Additionally, $\boldsymbol{s}_j \in \mathbb{R}^{6,1}$ represents the vector that groups the variables on the right side of each equation. The ideal value of each variable is unified as r_w for distance information and 0 for angle information.

If the variable with the highest error among the six values belongs to the front-end wheel of the connection part, the front-end of the connection part is set as the control object. Conversely, if the error of the component at the rear-end of the connection part exceeds the threshold, the rear-end of the connection part is set as the control object. If any component exceeds the threshold at both ends of the connection part, the side with the wheel that has the smallest sensor distance information is set as the reference.

To determine the end condition of the recovery control, values $d_{l,i}$, $d_{r,i}$, and ${}^l\phi_i$ (${}^{-l}\phi_i$) related to the ground state of the wheel are used among the control variables. Initially, the robot executes the recovery control until the error between these values and their target values falls within a predefined threshold $\boldsymbol{e}_j$=$[e_l, e_r, e_\phi]^{\top} \in \mathbb{R}^{3,1}$. Subsequently, the recovery control is terminated after t_e seconds have elapsed while maintaining the error within the threshold range. t_e represents an arbitrary constant. It can be confirmed that the control variable has converged near the target value by waiting t_e second after the control variable error reaches the threshold range.

Under the requirements above, the system switches between propulsion control and recovery control. Fig.19 shows an overview of these operational transitions.

TABLE 2. Parameters employed in the experiment.

Parameter	Value
l[m]	0.0985
r_w[m]	0.052
m_c	9
a_s[m]	0.0980
ψ_{lim}[rad]	$\pi/2$
k_r	1
K_r	$\begin{bmatrix}1&0&0&0\\0&1&0&0\\0&0&1&0\\0&0&0&1\end{bmatrix}$
k_p	1
K_p	$\begin{bmatrix}1&0&0&0\\0&1&0&0\\0&0&1&0\\0&0&0&1\end{bmatrix}$
g_1	0.7
g_2	0.3
d_{h1}	0.272
d_{h2}	0.272
v[m/s]	0.015
A[m]	0.15
T[s]	90
t_e	1
s_j	$[0.004, 0.004, 10\pi/180, 0.004, 0.004, 10\pi/180]^{\top}$
e_j	$[0.003, 0.003, 8\pi/180]^{\top}$

IV. EXPERIMENT

A. EXPERIMENTAL SETUP

To validate the effectiveness of the proposed method, we conducted experiments using an actual robot as shown in Fig.20.

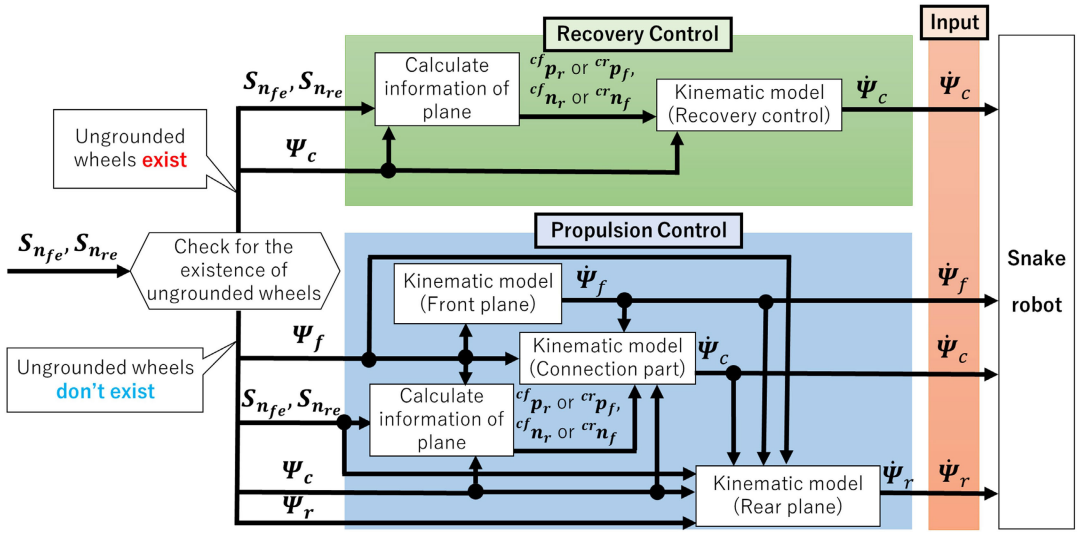

FIGURE 19. Transition diagram to control input calculation.

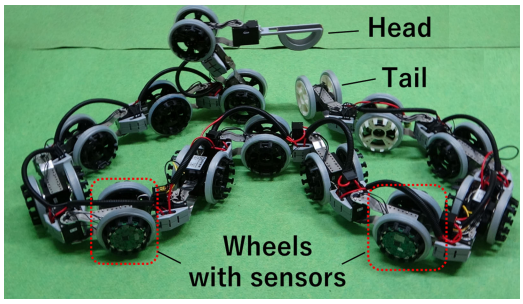

FIGURE 20. The snake robot used in the experiment.

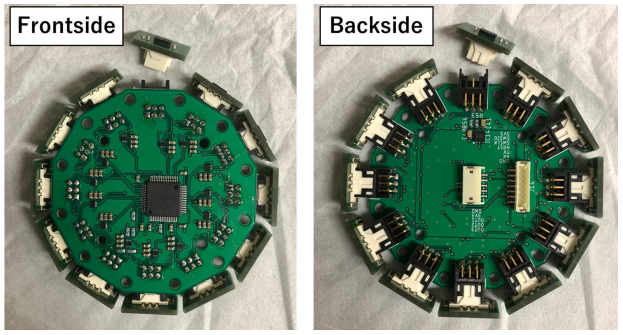

(a) External appearance of the sensor

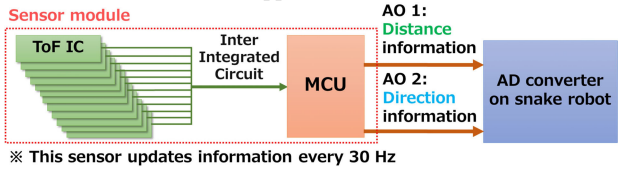

(b) Sensor Composition

FIGURE 21. Proximity sensor utilized in the experiment.

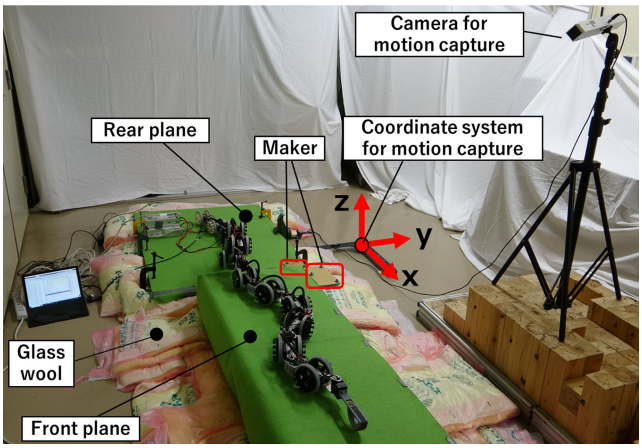

FIGURE 22. Experiment Environment.

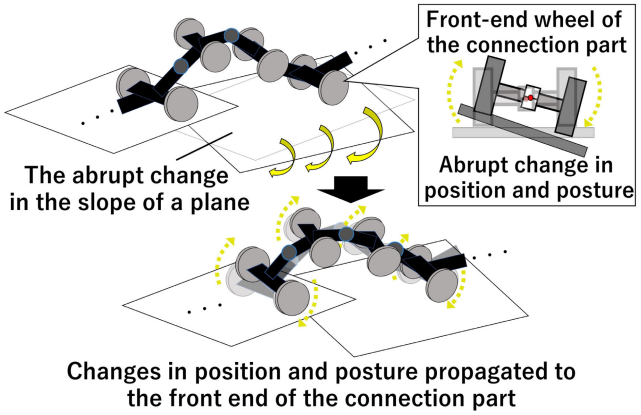

FIGURE 23. Propagation of robot position and posture changes.

This robot has 27 joints and 14 wheels. The proximity sensor is affixed to the wheel pair of both ends of the connection part. Fig.21 shows the sensor employed in the experiment, comprising a Micro-Control Unit (STM32L476RG)

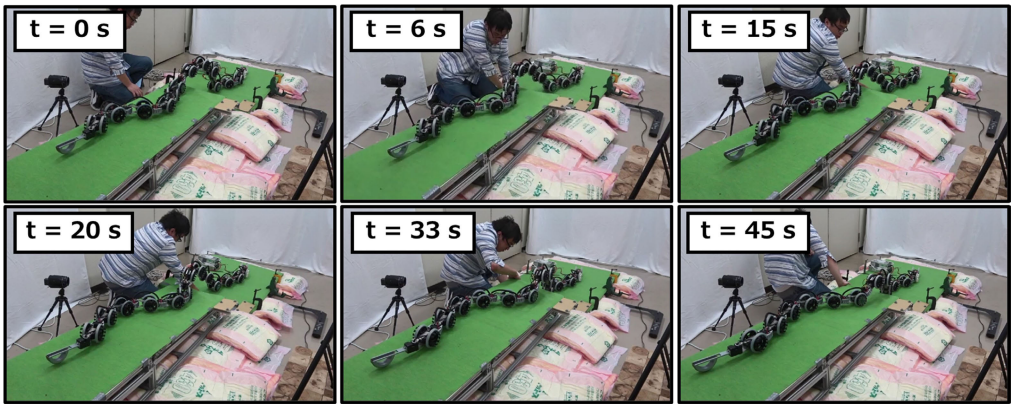

(a) Appearance of the experiment

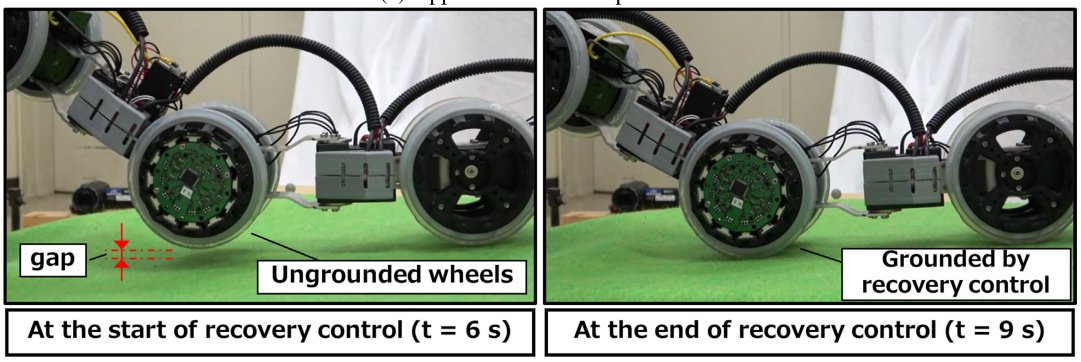

(b) Contact state of wheels with plane before and after the recovery control

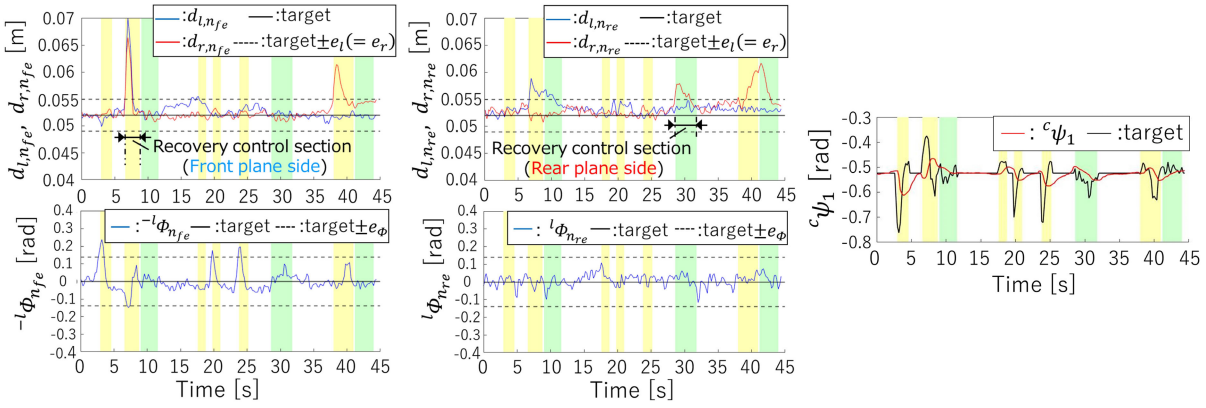

(c) Time variation of $d_{l,n_{fe}}$, $d_{r,n_{fe}}$, and $^{-l}\phi_{n_{fe}}$ (d) Time variation of $d_{l,n_{re}}$, $d_{r,n_{re}}$, and $^{l}\phi_{n_{re}}$ (e) Time variation of $^{c}\psi_1$

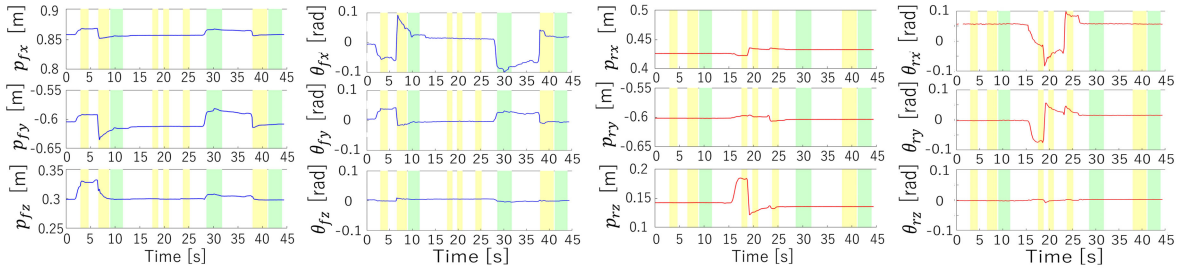

(f) Position of the front plane at each time (g) Attitude of the front plane at each time (h) Position of the rear plane at each time (i) Attitude of the rear plane at each time

FIGURE 24. Experimental results in case of success.

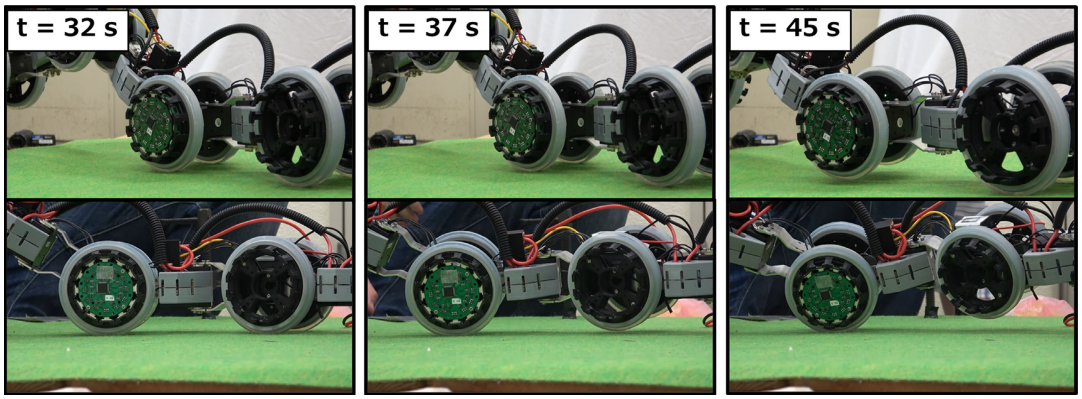

(a) Appearance of the experiment : The upper figure shows the front-end of the connection part and the lower figure shows the rear-end of the connection part.

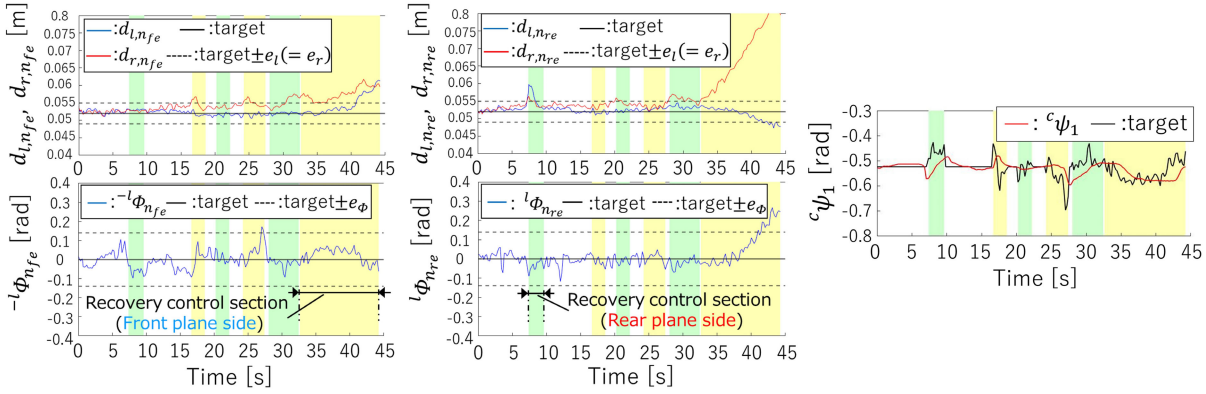

(b) Time variation of $d_{l,n_{fe}}$, $d_{r,n_{fe}}$, and $-{}^{l}\phi_{n_{fe}}$ (c) Time variation of $d_{l,n_{re}}$, $d_{r,n_{re}}$, and ${}^{l}\phi_{n_{re}}$ (d) Time variation of ${}^{c}\psi_1$

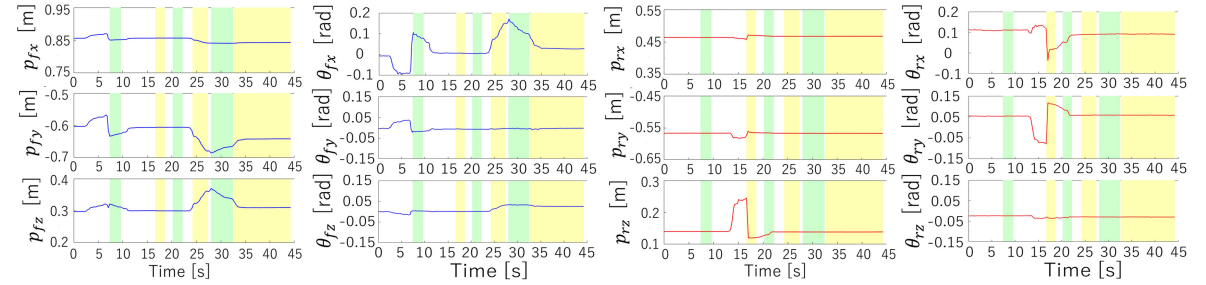

(e) Position of the front plane at each time (f) Attitude of the front plane at each time (g) Position of the rear plane at each time (h) Attitude of the rear plane at each time

FIGURE 25. Experimental results in case of failure.

and 12 Time of Flight elements (VL6180x) arranged along the circumference. These ToF elements to be employed experience diminished accuracy when the measurement distance is less than 10 mm. Therefore, the sensor is circular with a radius of 35 mm, which is at least 10 mm smaller than the wheel radius. This ensures that the measurement distance is always more than 10 mm. The MCU and ToF elements are detachable with connectors, facilitating measurement range adjustment and ToF element replacement in case of failure. Considering this condition and physical interference, the ToF elements around the circumference were set at 12. The robot employs servo motors (Dynamixel XM540) equipped with a 3-channel AD converter, streamlining wiring complexities. The MCU processes information from the 12 ToF elements, converting it into the sensor information shown in Fig.1, subsequently transmitting it as an analog voltage. The motor receives this information, A/D measured at 12-bit resolution, and transmits it to the control computer. As mentioned previously, sensor information errors are reduced through a moving average filter and a predetermined offset value.

In this experiment, we set n_{fe} to 6, n_{re} to 10. The robot started its motion from a position straddling two planes, executing movements until just before the next propagation

of the connection part. The robot's control frequency is 0.2 s. The target relative velocity of the robot head at time t is defined as $\dot{\boldsymbol{w}}_d = [\dot{x}_{hd}(t), \dot{y}_{hd}(t), \dot{\theta}_{hd}]^\top = [v, (2\pi A/T)\cos(2\pi t/T), 0]^\top$. v is the propulsive velocity of the head, A is the amplitude of the propulsive trajectory, and T is the period of the propulsive trajectory.

Fig.22 shows the experimental environment, featuring two non-parallel planes with glass wool underneath them. External forces can incline the plane on the glass wool. Manually moving each plane during robot motion realizes a variable two-plane environment. Motion capture markers are affixed to the left edge of each plane, measuring the plane's position and orientation. Table 2 outlines the control parameters used in the experiment.

B. RESULT

Under these conditions, the experiment results are shown in Fig.24. As shown in Fig.24(a), the robot successfully propelled itself through the two variable planes without significant problems.

Fig.24(c–i) reveals that the error of the control variable at both ends of the connection part increased when the plane's inclination changed, such as at $t = 6, 28, 38$ s. At $t = 28$ s, the control variable error at the rear-end of the connection part increased, despite the front plane changing. Fig.23 suggests that this error is attributed to the propagation of positional and orientational alterations from the rear plane's wheel to the front plane. With the heightened control variable error, the number of ungrounded wheels on the plane increased, as illustrated in Fig.24(b). However, upon sensor detection of an ungrounded wheel, the robot executed recovery control, reducing the control variable error within the defined threshold. Subsequently, the robot resumed propulsion once the ungrounded wheels were properly grounded.

In Fig.24(c–i) at $t = 40$ s, the control variable error at the rear-end of the connection part increased during the recovery control of the front-end, despite the stationary plane. This anomaly is attributed to the excessive pushing of the front-end wheel against the front plane, causing the rear-end wheel to lift due to the reaction force. The recovery control of the front-end ends and accordingly, the recovery control of the rear-end started. Consequently, the robot successfully traversed between the two variable planes, ensuring all wheels on the plane remained grounded.

Fig.25 shows that the example of the robot failed in recovery control. This result was caused when the control object was not promptly switched when the reference wheel was lifting from the rear plane. At $t = 33 - 37$ s in Fig.25(b), the change in $d_{r,n_{fe}}$ stagnated near the threshold boundary, leading to prolonged recovery control completion. At this time, the rear-end wheel of the connection part, serving as the reference, tilted due to the reaction force. The robot nearly overturned by $t = 37 - 45$ s.

In the proposed method, the control part is not switched unless the end requirement of the recovery control is satisfied, even if the reference wheel becomes ungrounded. This model based on kinematics, assumes the axle center of the reference wheel as a fixed reference point. Therefore, the control cannot accommodate temporal variations in the reference point or the risk of the robot tipping over.

Situations such as Pattern 3 in Fig.6 are excluded from the assumed conditions due to potential violations of the fixed reference point assumption. The ground condition of the reference wheel became worse because the recovery control was executed under these conditions. Addressing this necessitates refining the control switching requirements to allow control object switching when the reference wheel becomes ungrounded, or enhancing the control model to account for dynamic effects.

V. CONCLUSION

This paper proposed a control method for a snake robot to move in a two-plane environment with changing information of plane. In the method, information of plane is estimated based on data acquired from proximity sensors. By combining the sensor information with propulsion and recovery control, the robot can propel itself through the environment while ensuring all wheels remain grounded on the plane. The main contribution of the proposed method is to enable the snake robot to move between two variable planes, which has not been solved in previous studies. Experiments using an actual snake robot validated the effectiveness of the proposed method. This paper verifies the motion of the robot until just before the propagation of the connection part. These results suggest that the snake robot can achieve traversal between the two variable planes by using sensor information to determine the optimal timing of the connection part propagation. In this study, a robot with the configuration shown in Fig.1(a) was adopted. However, the proposed method can be applied to a wheeled snake robot with different joint configurations, as long as the plane part has a joint configuration with degrees of freedom for undulating motion for propulsion and the connection part has degrees of freedom for maintaining proper contact of the wheels, respectively. We have also established a control method for propulsive motion that follows a target trajectory for two variable planes with the proposed method. Therefore, we expect that autonomous moving between two variable planes can be achieved if we can estimate the self-position of the head, which is the control point, and generate a target for the head's trajectory. The generation of the target trajectory when moving between two planes and the 3D self-position estimation for detecting the position and orientation of the robot head can be achieved by applying the methods used for general mobile robots. In addition, to traverse the assumed environment, the robot requires not only motion for propulsion between the two planes, but also motion for approach to the next plane, as shown in (A) and (B) of Fig.3. The control method and target trajectory generation in this motion could be realized by applying the semiautonomous climbing method for two parallel planes proposed by Kon [6]. By implementing these

components in a robot, the robot may be able to perform autonomous moving between two variable planes.

However, there are still issues that need to be solved for real-world operations. The design of energy-efficient machines and systems is an important factor in the actual operation of snake robots. Therefore, future works will require proposals for actual robots and systems that can both move between two variable planes and achieve high energy efficiency. In addition, the contact condition of the wheels in this method is defined based on the assumption that the two footings are both flat surfaces. Therefore, the proposed method is not yet applicable to footings with otherwise flat surfaces. In a real environment, it may be necessary to transfer to footings with complex shapes, such as rubble at a disaster site. To operate in real environments, it will be necessary to define wheel contact conditions that can be applied to environments other than flat surfaces, and incorporate them into the proposed method. Other than these, future work includes proposing a control method that can be applied to situations in which both ends of the connection part are improperly grounded.

REFERENCES

[1] P. Prautsch, T. Mita, and T. Iwasaki, "Analysis and control of a gait of snake robot," *IEEJ Trans. Ind. Appl.*, vol. 120, no. 3, pp. 372–381, 2000.

[2] F. Matsuno and K. Suenaga, "Control of redundant 3D snake robot based on kinematic model," in *Proc. IEEE Int. Conf. Robot. Automat.*, Sep. 2003, pp. 2061–2066.

[3] M. Yamakita, M. Hashimoto, and T. Yamada, "Control of locomotion and head configuration for 3D snake robot," *Robot. Soc. Jpn.*, vol. 22, no. 1, pp. 61–67, 2004.

[4] M. Tanaka, K. Kon, and K. Tanaka, "Range-sensor-based semiautonomous whole-body collision avoidance of a snake robot," *IEEE Trans. Control Syst. Technol.*, vol. 23, no. 5, pp. 1927–1934, Sep. 2015.

[5] F. Matsuno and K. Mogi, "Redundancy controllable system and control of snake robots based on kinematic model," in *Proc. 39th IEEE Conf. Decis. Control*, Dec. 2000, pp. 4791–4796.

[6] K. Kon, M. Tanaka, and K. Tanaka, "Mixed integer programming-based semiautonomous step climbing of a snake robot considering sensing strategy," *IEEE Trans. Control Syst. Technol.*, vol. 24, no. 1, pp. 252–264, Jan. 2016.

[7] M. Tanaka and K. Tanaka, "Control of a snake robot for ascending and descending steps," *IEEE Trans. Robot.*, vol. 31, no. 2, pp. 511–520, Apr. 2015.

[8] Q. Fu and C. Li, "Robotic modelling of snake traversing large, smooth obstacles reveals stability benefits of body compliance," *Roy. Soc. Open Sci.*, vol. 7, no. 2, Feb. 2020, Art. no. 191192.

[9] T. Kamegawa, T. Harada, and A. Gofuku, "Realization of cylinder climbing locomotion with helical form by a snake robot with passive wheels," in *Proc. IEEE Int. Conf. Robot. Autom.*, May 2009, pp. 3067–3072.

[10] M. Nakajima, M. Tanaka, K. Tanaka, and F. Matsuno, "Motion control of a snake robot moving between two non-parallel planes," *Adv. Robot.*, vol. 32, no. 10, pp. 559–573, 2018.

[11] K. Lipkin, I. Brown, A. Peck, H. Choset, J. Rembisz, P. Gianfortoni, and A. Naaktgeboren, "Differentiable and piecewise differentiable gaits for snake robots," in *Proc. IEEE/RSJ Int. Conf. Intell. Robots Syst.*, Oct./Nov. 2007, pp. 1864–1869.

[12] D. Rollinson and H. Choset, "Gait-based compliant control for snake robots," in *Proc. IEEE Int. Conf. Robot. Autom.*, May 2013, pp. 5138–5143.

[13] T. Takemori, M. Tanaka, and F. Matsuno, "Gait design for a snake robot by connecting curve segments and experimental demonstration," *IEEE Trans. Robot.*, vol. 34, no. 5, pp. 1384–1391, Oct. 2018.

[14] T. Takemori, M. Tanaka, and F. Matsuno, "Adaptive helical rolling of a snake robot to a straight pipe with irregular cross-sectional shape," *IEEE Trans. Robot.*, vol. 39, no. 1, pp. 437–451, Feb. 2023.

[15] C. Gong, M. Tesch, D. Rollinson, and H. Choset, "Snakes on an inclined plane: Learning an adaptive sidewinding motion for changing slopes," in *Proc. IEEE/RSJ Int. Conf. Intell. Robots Syst.*, Sep. 2014, pp. 1114–1119.

[16] R. Watanabe and M. Tanaka, "Principle of object support by Rope deformation and its application to Rope climbing by snake robot," *Adv. Robot.*, vol. 37, no. 9, pp. 591–602, 2023.

[17] J. Bae, M. Kim, B. Song, M. Jin, and D. Yun, "Snake robot with driving assistant mechanism," *Appl. Sci.*, vol. 10, no. 21, p. 7478, 2020.

[18] H. Yamada and S. Hirose, "Study of active cord mechanism—Approximations to continuous curves of a multi-joint body," *J. Robot. Soc. Jpn.*, vol. 26, no. 1, pp. 110–120, 2008.

[19] L. Pfotzer, M. Staehler, A. Hermann, A. Roennau, and R. Dillmann, "KAIRO 3: Moving over stairs & unknown obstacles with reconfigurable snake-like robots," in *Proc. Eur. Conf. Mobile Robots (ECMR)*, Sep. 2015, pp. 1–6.

[20] K. Kouno, H. Yamada, and S. Hirose, "Development of active-joint active-wheel high traversability snake-like robot ACM-R4.2," *J. Robot. Mechtron.*, vol. 25, no. 3, pp. 559–566, 2013.

[21] M. Tanaka, M. Nakajima, Y. Suzuki, and K. Tanaka, "Development and control of articulated mobile robot for climbing steep stairs," *IEEE/ASME Trans. Mechatronics*, vol. 23, no. 2, pp. 531–541, Apr. 2018.

[22] D. S. Apostolopoulos, M. D. Wagner, B. N. Shamah, L. Pedersen, K. Shillcutt, and W. L. Whittaker, "Technology and field demonstration of robotic search for Antarctic meteorites," *Int. J. Robot. Res.*, vol. 19, no. 11, pp. 1015–1032, 2000.

[23] M. Heverly, J. Matthews, J. Lin, D. Fuller, M. Maimone, J. Biesiadecki, and J. Leichty, "Traverse performance characterization for the Mars Science Laboratory rover," *J. Field Robot.*, vol. 30, no. 6, pp. 835–846, 2013.

[24] X. Liang, M. Xu, L. Xu, P. Liu, X. Ren, Z. Kong, J. Yang, and S. Zhang, "The AmphiHex: A novel amphibious robot with transformable leg-flipper composite propulsion mechanism," in *Proc. IEEE/RSJ Int. Conf. Intell. Robots Syst.*, Oct. 2012, pp. 3667–3672.

[25] T. Matsuzawa, A. Koizumi, K. Hashimoto, X. Sun, S. Hamamoto, T. Teramachi, S. Kimura, N. Sakai, and A. Takanishi, "Crawling gait for four-limbed robot and simulation on uneven terrain," in *Proc. IEEE-RAS 16th Int. Conf. Humanoid Robots (Humanoids)*, Nov. 2016, pp. 1270–1275.

[26] H.-M. Joe and J.-H. Oh, "A robust balance-control framework for the terrain-blind bipedal walking of a humanoid robot on unknown and uneven terrain," *Sensors*, vol. 19, no. 19, p. 4194, Sep. 2019.

[27] Y. She, C. J. Hurd, and H.-J. Su, "A transformable wheel robot with a passive leg," in *Proc. IEEE/RSJ Int. Conf. Intell. Robots Syst. (IROS)*, Sep. 2015, pp. 4165–4170.

[28] C. Creager, K. Johnson, M. Plant, S. Moreland, and K. Skonieczny, "Push–pull locomotion for vehicle extrication," *J. Terramech.*, vol. 57, pp. 71–80, Feb. 2015.

[29] K. Iagnemma, A. Rzepniewski, S. Dubowsky, and P. Schenker, "Control of robotic vehicles with actively articulated suspensions in rough terrain," *Auton. Robots*, vol. 14, no. 1, pp. 5–16, 2003.

[30] K. Tadakuma, R. Tadakuma, K. Nagatani, K. Yoshida, S. Peters, M. Udengaard, and K. Iagnemma, "Crawler vehicle with circular cross-section unit to realize sideways motion," in *Proc. IEEE/RSJ Int. Conf. Intell. Robots Syst.*, Sep. 2008, pp. 2422–2428.

[31] K. Ohno, S. Morimura, S. Tadokoro, E. Koyanagi, and T. Yoshida, "Semi-autonomous control system of rescue crawler robot having flippers for getting over unknown-steps," in *Proc. IEEE/RSJ Int. Conf. Intell. Robots Syst.*, Oct./Nov. 2007, pp. 3012–3018.

[32] E. Rohmer, K. Ohno, T. Yoshida, K. Nagatani, E. Konayagi, and S. Tadokoro, "Integration of a sub-crawlers' autonomous control in quince highly mobile rescue robot," in *Proc. IEEE/SICE Int. Symp. Syst. Integr.*, Dec. 2010, pp. 78–83.

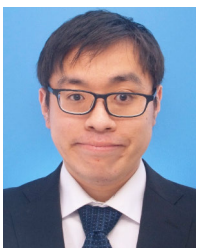

SHUNTA SUYAMA received the B.Eng. degree from the Department of Mechanical and Intelligent Systems Engineering, The University of Electro-Communications, Tokyo, Japan, in 2022, where he is currently pursuing the M.Eng. degree.

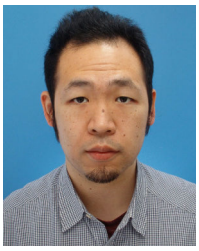

MIZUKI NAKAJIMA (Member, IEEE) received the B.Eng., M.Eng., and Ph.D. degrees in engineering from the Department of Mechanical and Intelligent Systems Engineering, The University of Electro-Communications, in 2014, 2016, and 2020, respectively. He is currently an Assistant Professor with the Department of Robotics and Mechatronics, School of Science and Technology for Future Life, Tokyo Denki University. His research interests include the development and control of snake robots.

HIKARU ARITA (Member, IEEE) received the B.Eng., M.Eng., and Ph.D. degrees in engineering from The University of Electro-Communications, Tokyo, Japan, in 2012, 2014, and 2019, respectively. He was with several institutions, including OMRON Corporation, Kyoto, Japan, from 2014 to 2016, and Ritsumeikan University, where he was an Assistant Professor, from 2019 to 2022. He is currently an Assistant Professor with Kyushu University, Fukuoka, Japan. His research interests include proximity sensors and sensor-based control.

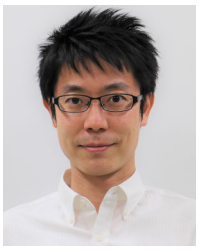

MOTOYASU TANAKA (Member, IEEE) received the B.Eng., M.Eng., and Ph.D. degrees in engineering from the Department of Mechanical Engineering and Intelligent Systems, The University of Electro-Communications, Tokyo, Japan, in 2005, 2007, and 2009, respectively. From 2009 to 2012, he was with the Canon Inc., Tokyo. He is currently a Professor with the Department of Mechanical and Intelligent Systems Engineering, The University of Electro-Communications. His research interests include biologically inspired robotics and dynamic-based nonlinear control. He was a recipient of the IEEE Robotics and Automation Society Japan Chapter Young Award from the IEEE Robotics and Automation Society Japan Chapter, in 2006, and the Best Poster Award at SWARM2015: The First International Symposium on Swarm Behavior and Bio-Inspired Robotics, Kyoto, Japan, in 2015.